Plasmon Coupling in Silver Nanocube Dimers: Resonance Splitting Induced by Edge Rounding

Nadia Grillet, Delphine Manchon, Franck Bertorelle, Christophe Bonnet, Michel Broyer, Emmanuel Cottancin, Jean Lermé, Matthias Hillenkamp, and Michel Pellarin*

Laboratoire de Spectrométrie Ionique et Moléculaire (UMR 5579) 43, CNRS, Université de Lyon, Université Lyon 1, Bld du 11 Novembre 1918, 69622 Villeurbanne Cedex, France

ABSTRACT Absolute extinction cross sections of individual silver nanocube dimers are measured using spatial modulation spectroscopy in correlation with their transmission electron microscopy images. For very small interparticle distances and an incident light polarized along the dimer axis, we give evidence for a clear splitting of the main dipolar surface plasmon resonance which is found to be essentially induced by cube edge rounding effects. Supported by discrete dipole approximation and finite element method calculations, this phenomenon highlights the high sensitivity of the plasmonic coupling to the exact shape of the effective capacitor formed by the facing surfaces of both particles, especially in the regime of very close proximity.

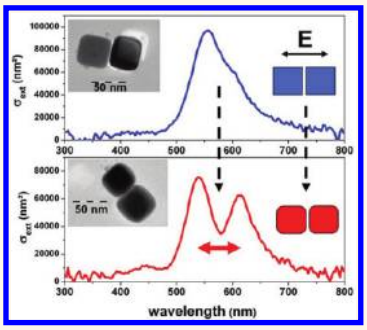

KEYWORDS: plasmon coupling · nanocube dimers · silver nanoparticles · single nanoparticle spectroscopy · DDA calculations

The peculiar optical response of metal nanoparticles dominated by their localized surface plasmon resonance (LSPR) is responsible for a selective spectral dependence of absorbed and scattered light[1] and for a large local electromagnetic field enhancement close to the nanoparticle surface.[2,3] The specific far-field and near-field features of their LSPR are known to be closely dependent on the particle size, shape, chemical composition, and dielectric environment.[4] Noble metal particles have then been rapidly considered as ideal candidates for performing high sensitivity detection[5,6] and spectroscopy of molecules suitably attached to their surface.[7] A higher flexibility in tuning the LSPR features can be obtained by considering several closely spaced nanoparticles. Because of electrostatic coupling, the interaction between individual plasmons strongly modifies the optical response as soon as the surface-to-surface distance (*d*) between particles is of the order of their lateral size (*L*). In the simple case of nanoparticle dimers excited by an electromagnetic wave linearly polarized along the interparticle axis, the most striking effect is a shift of the resulting LSPR toward low energies when the interparticle spacing is reduced.[8−12] This shift follows a universal scaling law as a function of the dimensionless parameter *d*/*L* (quasi-exponential behavior) and has given birth to the concept of "plasmon ruler" that may be used to infer the length of a molecular chain connecting functionalized nanoparticles.[13,14]

For the past few years, plasmonic coupling between metal nanoparticles has been a major issue with the idea of tailoring the properties of metallic nanoantennas by taking advantage of the very large and localized electromagnetic field enhancement in the interparticle gap region.[15] This is illustrated in the field of molecular fluorescence detection,[16] Raman scattering measurement,[17,18] or biochemical sensing[19] for instance. Pioneering studies on plasmon coupling have mostly concerned nanoparticles with simple and regular geometries (spheres, cylindrical dots, *etc.*). They have been further extended to more complex objects designed by colloidal chemistry[20,21] or nanolithography engraving,[22,23] covering an increasing variety of nanoparticle shapes and organizations. A recent and exhaustive review in the case of silver nanostructures is given by Xia *et al.*[24] Besides the interparticle distance, the relative particle orientation is also a crucial parameter since it finely controls the effective capacitance of the two facing metallic surfaces and the resulting electrostatic coupling between surface charge distributions.[12,25−27]

The case of very close nanoparticles, near the contact limit, is less discussed and remains challenging.[25,28] For very short

* Address correspondence to pellarin@lasim.univ-lyon1.fr.

Received for review June 15, 2011 and accepted November 16, 2011.

Published online November 16, 2011
10.1021/nn2041329

interparticle distances, the plasmon ruler model cannot be applied any longer. The strong interaction between surface charges and their complex piling up in the gap region ensure the coupling of an increasing number of low symmetry collective oscillation modes and the development of a complex plasmonic response.[29] In this respect, we report on experiments that clearly demonstrate the influence of the exact nanoantenna geometry, in the particular case of silver dimers consisting of nanocubes with various degrees of edge smoothness. We will show that the nature and strength of the plasmonic coupling in the regime of closest proximity is dominated by the ratio between interparticle separation *d* and surface curvatures rather than between separation and nanoparticle size. In particular, we give evidence for an unexpected splitting of the main dipolar surface plasmon resonance due to cube edge rounding effects.

RESULTS AND DISCUSSION

Single Nanocube Spectroscopy: Experiment and Simulations. Absolute optical extinction spectra of individual nanoparticles are measured by a high sensitivity spectrophotometer operating on the basis of the spatial modulation spectroscopy technique. Corresponding images are obtained by transmission electron microscopy (TEM). Figure 1a shows the extinction cross sections of two nanocubes (M1 and M2). Their projected images on the substrate plane normal to the electron beam are roughly square (edge lengths $L = 55$ nm and $L = 41$ nm for M1 and M2, respectively). M1 and M2 can be considered as cubic particles if their nonmeasurable dimension in the direction of the electron beam is reasonably assumed to be close to the lateral size. M1 and M2 extinction spectra are similar. They show a main resonance at about 440 nm and a shoulder on their short wavelength side. They are found to be independent of the linear polarization direction as expected for objects that remain unchanged by a $\pi/2$ rotation around the incident light beam axis. The difference in maximum peak intensities mirrors the difference in particle sizes. As it can be noticed from TEM micrographs, silver particles are not always shaped as perfect cubes. To simply account for such deviations and in the perspective of performing optical response calculations, we will consider cube geometries with various degrees of edge rounding. As shown in Figure 1b, the sharp edges of length *L* are replaced by quarter cylinders of radius r_e set tangent to the cube faces. Moreover, the corners can be eventually rounded off and replaced by eight spheres of the same radius ($r_c = r_e$). On a geometrical point of view, it is not possible to decide between both possibilities from the TEM images. They only inform about the rounding of the four edges perpendicular to the substrate. Although curvature radii are not exactly the same,

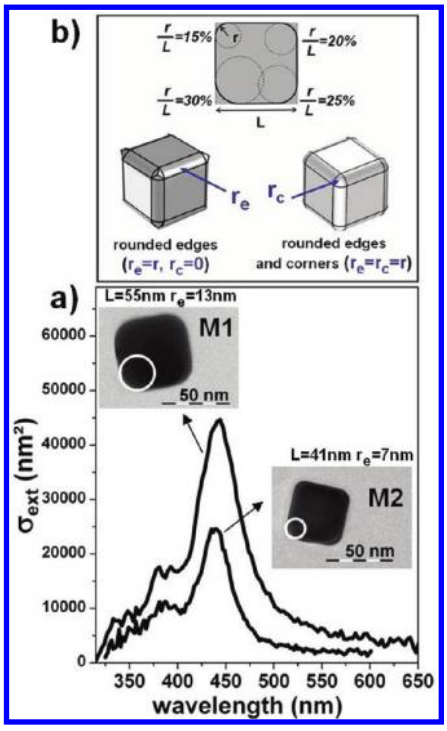

Figure 1. (a) Absolute extinction spectra of single silver cubes (monomers M1 and M2). Average side lengths (*L*) and edge curvatures (white circles with radius r_e) are determined for both cubes from their TEM images (50 nm scale bar). (b) Proposed geometrical structures for smoothed cubes. Edges can be replaced by quarter cylinders (radius r_e), with or without additional corner rounding (radius $r_c = r_e$). For both cases, the topmost drawing gives a visual impression for increasing levels of edge smoothing (r/L).

a common r_e (r_c) value will be assumed in the following for every edge (corner) and will be taken as the mean value deduced from TEM views. Effective edge roundings of about 13 and 7 nm are thus estimated for M1 and M2, respectively (Figure 1a).

Numerical simulations of a single nanocube extinction spectrum using the discrete dipole approximation (DDA) or a finite element method (FEM) are shown in Figure 2 in the particular case of M2 ($L = 41$ nm). We have considered three different geometries depending on the level of edge and corner rounding. For a sharp edge cube (Figure 2b), a weak smoothing ($r_e = r_c = 0.5$ nm) is necessary to remove spurious geometrical singularities in FEM calculations. The particle is assumed to be embedded in a homogeneous dielectric medium with refractive index $n_{eff} = 1.15$ (see Materials and Methods). The present calculations are in line with those already published in the literature for large perfect silver cubes.[30−33] DDA and FEM give here similar results, and only resonances labeled 2 and 3 are slightly shifted. Compared to spheres, the LSPR fragmentation is a direct consequence of symmetry lowering. The multimodal structure clearly mirrors the one discussed in theoretical studies on small cubes in the quasi-static approximation.[34,35] For each of the wavelengths corresponding to the most apparent

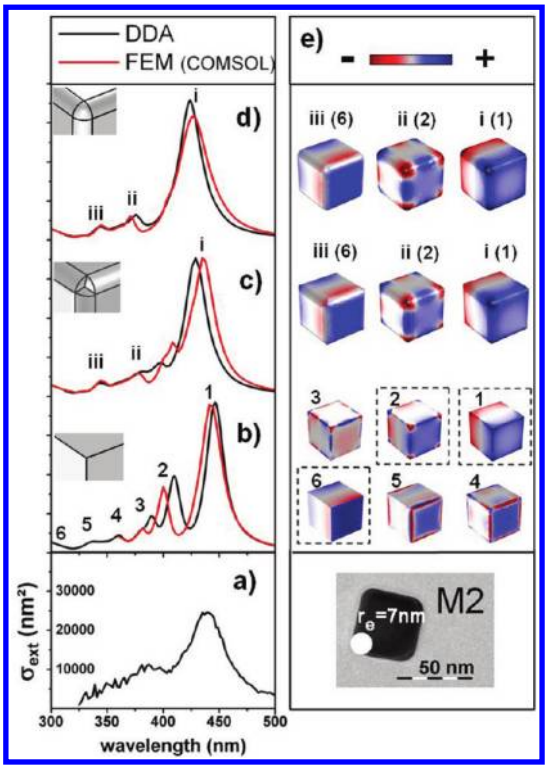

Figure 2. (a–d) Comparison between experimental (a) and simulated extinction cross sections (b–d) for nanocube M2 (L = 41 nm). Calculations are performed using both DDA (black curves) and FEM (red curves) in the case of perfect (b), edge rounded ((c) with r_e = 7 nm) and both edge and corner rounded cubes ((d) with $r_e = r_c$ = 7 nm). The FEM simulation in (b) is made for a weak smoothing ($r_e = r_c$ = 0.5 nm). The effective matrix refractive index is n_{eff} = 1.15 (b) or n_{eff} = 1.25 (c–d). (e) Surface charge distributions calculated by FEM at the most marked resonances in the corresponding simulated spectra on the left. The scale for surface charge densities is only indicative since, case by case, the color range has been arbitrarily truncated to obtain more contrasted images at the cost of spurious saturation effects.

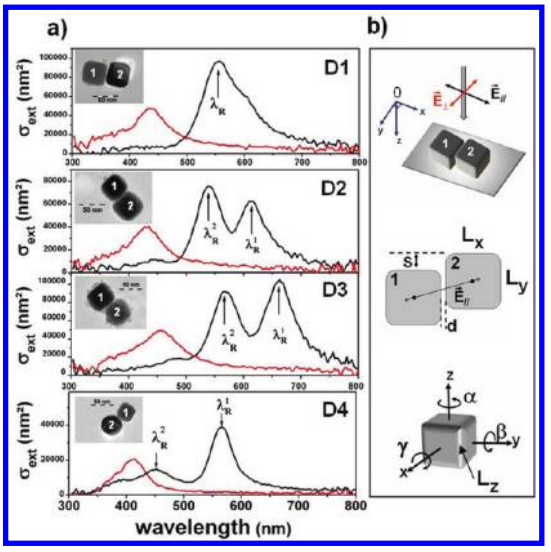

Figure 3. (a) Absolute extinction spectra of single silver nanocube dimers for an incident electric field polarized along (black curves) or perpendicular (red curves) to the interparticle axis. For a longitudinal excitation, the two main resonances are labeled λ_R^1 and λ_R^2. TEM images are all drawn on the same scale (50 nm scale bar). (b) Schemes showing the excitation setup with reference to the Oxyz laboratory frame (top) and the main geometric parameters characterizing a nanocube dimer (middle and bottom): d is the minimum distance between adjacent cube faces; S is the lateral shift in the y direction; α, β, and γ are the Euler angles describing a possible cube rotation in the Oxyz frame. Nonperfectly cubic particles are characterized by their side lengths L_x, L_y, and L_z (edge rounding parameters are defined in Figure 1b).

resonances (1–6 in Figure 2b), surface charge distributions calculated with FEM are displayed in Figure 2e. They have the same structure as those obtained for small particles studied in the electrostatic limit by Zhang *et al.*[36]

When edges (and eventually corners) are rounded, calculated spectra are broader and slightly red-shifted as compared to the case of perfect cubes. The effective matrix refractive index has been arbitrarily increased (n_{eff} = 1.25) for a better correspondence between experiment and simulations shown in Figure 2c,d. For both the edge and corner rounded cube (Figure 2d), DDA and FEM calculations are almost identical and only three resonances (i, ii, iii) can be clearly distinguished. From the inspection of their corresponding surface charge distributions (Figure 2e), they can be, respectively, related to the perfect cube resonances 1, 2, and 6. For the edge rounded cube (Figure 2c), simulated spectra differ from those obtained with an additional corner rounding (Figure 2d), especially in the region of resonance ii, although surface charge distributions are similar. It must be noted that in mode ii, as in mode 2, the nodes of the charge distribution are located at the cube corners. The high sensitivity of this resonance to the exact corner shape is certainly at the origin of the differences between spectra in Figure 2c,d. In the absence of an additional rounding, corners have a singular geometry resulting from the intersection of three cylindrical edges (inset in Figure 2c). FEM is not suited to account for such structural discontinuities, and in DDA, the finite mesh size of the dipole array induces a spurious "roughness" of the outermost dipole especially in these singular corner regions. This may also explain why FEM and DDA calculations in Figure 2c deviate one from each other in the region of resonance ii. Nevertheless, simulations of the optical response of silver nanocubes assuming smoothed edges or corners are consistent with experimental measurements even if optical spectra obtained in previous experiments[37,38] are somewhat different from those reported in this work. This discrepancy certainly finds its origin in the different nature and thickness of the substrates used in both experiments. Electrostatic mirroring effects at the air–dielectric interface were invoked to explain the hybridization between bright dipolar and dark quadrupolar modes in these studies.[36] They cannot be excluded but may be less important here.

TABLE 1. Geometrical Parameters of Silver Cube Dimers Obtained from TEM Images

		in plane edge lengths[a,c]		out of plane edge length[b]			edge/corner radius[c]	orientation[e]
		L_x (nm)	L_y (nm)	L_z (nm)	lateral shift[c] S(nm)	spacing d_{app}[c,d] (nm)	r (nm)	α ($\beta = 0°, \gamma = 0°$)
dimer D1	P1	47	47	(47)	+5	1.75	7	0°
	P2	45	49	(47)			9	2°
dimer D2	P1	43	47	(45)	−5	(−2.3)	11	0°
	P2	51	51	(51)			9	−2°
dimer D3	P1	51	59	(55)	+7	(−3)	12	0°
	P2	53	57	(55)			13	1°
dimer D4	P1	33	33	(33)	−11	1.5	8	0°
	P2		$R = 21$					

[a] Rounded to the nearest odd integer. [b] L_z cannot be measured and is taken as the mean value between L_x and L_y. [c] ±2% relative accuracy. [d] Negative values indicate an apparent overlapping. [e] ±1° accuracy.

Optical Response of Single Nanocube Dimers: Evidence for a LSPR Splitting. Extinction spectra of several silver nanocube dimers obtained for orthogonal directions of the incident electric field polarization are shown in Figure 3a together with the corresponding TEM images (D1−D4). The excitation setup is schematized at the top of Figure 3b. The nanocubes and their relative arrangement within each dimer can be different. Some of their characteristic geometrical parameters defined either in Figure 1b or in Figure 3b can be obtained by inspecting TEM images. They are summarized in Table 1. For example, both cubes in dimer D1 have a similar size ($L \cong 47$ nm). They are slightly shifted in the substrate plane, and their apparent separation is $d_{app} = 1.75$ nm. For a transverse excitation, the electrostatic coupling between particles is predicted to be of minor importance. The LSPR profile is then close to that of the single nanocube with an expected double intensity. For a longitudinal excitation, the extinction spectrum consists of a single peak which is more intense and shifted toward longer wavelengths ($\lambda_R = 565$ nm). It seems very similar to the one of spherical particle dimers, and the LSPR could be described, in a first attempt, as resulting from the coupling of individual plasmon modes of "dipolar" character. To our knowledge, optical experiments on silver nanocube dimers are rather scarce,[30,39,40] and this is the first observation of their far-field optical response. It must be noted that scattering spectroscopy of gold nanocube dimers was previously reported by Chen *et al.*[41] As compared to the present study, the use of unpolarized excitation light was, however, not suitable to highlight intrinsic modifications of the LSPR structure due to electrostatic coupling effects.

For a transverse excitation, extinction spectra of dimers D2 and D3 peak in the 420−450 nm range, just as for D1. Dispersions in the LSPR spectral location and broadening are not surprising since, in this configuration, the optical response of the dimer is close to the sum of the weakly correlated contributions of both particles which have different sizes and shapes. However, a striking feature for dimers D2 and D3 is the appearance of two distinct resonances (λ_R^1 and λ_R^2) that are not detected in the extinction spectrum of D1. This LSPR splitting differs from what is commonly established for dimers of spheres or cylindrical dots. The intensity and the spectral position of both resonances may vary from one dimer to another, which certainly reflects differences in their electrostatic coupling and local environment. Nevertheless, the ratio of both resonance frequencies λ_R^1/λ_R^2 is surprisingly quite well-defined and of the order of 1.15. This specific optical response should find its origin in morphological differences between D1 and D2 (D3). When they are close to each other, a slight mismatch between the electron beam axis and the normal to the substrate surface may give the impression that separate silver cubes are in contact (D2 and D3 for example). In the interparticle region, the cube edges are partially transparent to the electron beam and their contours can be outlined from TEM images. This is consistent with the presence of an underlying free space volume and shows that the contact is only apparent. On the interparticle axis, the separation distance d_{app} between overlapping cube edges can be arbitrarily defined as negative (D2 and D3 in Table 1). The value of d_{app} will be positive for clearly separated particles (D1 and D4 in Table 1). In general, d_{app} is nothing more than the difference between the actual interparticle distance d and the parallax shift. If this shift is similar whatever the dimer concerned, nanoparticles in dimers D2 and D3 are certainly much closer than in dimer D1. Moreover, D2 and D3 have smoother edges and corners. In some cases, TEM images indicate the presence of small particles surrounding the silver cubes. They are not impurities from the synthesis process but result from long exposures to the light beam during optical measurements (photochemical aging). If they are made of silver metal or silver oxide, the size of these grains is so small that they will only slightly modify the refractive index of the surrounding

dielectric medium (weakly absorbing or scattering layer), the dimer plasmonic properties remaining qualitatively unchanged. In the following, we will use numerical simulations to identify the physical origin of this unexplained splitting and try to quantify the influence of different geometrical parameters on its development. The special case for which one particle is clearly spherical (dimer D4) will be discussed afterward.

LSPR in Silver Nanocube Dimers: The Case of Perfect Cubes. In a classical approach, the plasmonic coupling in a nanoparticle pair results from the electrostatic interaction between the electron charge distributions induced on both facing surfaces. As established early by Prodan *et al.*, it can be modeled in analogy with molecular orbital theory describing the quantum states of diatomic molecules.[42] In the simple case of two identical particles showing a single LSPR (dipolar character for instance) and moved close one to each other, the degenerate plasmon will split into two hybridized bonding and antibonding modes in a way very similar to the degeneracy removal and level splitting in single level atomic systems. For a longitudinal excitation, the bright (bonding) mode is shifted to the low energy side and corresponds to the in-phase oscillation of both electron clouds. The collective oscillation is slowed by the electrostatic attraction between high charge densities of opposite sign sustained on the facing surfaces. For a transverse excitation, the charge accumulation in the capacitive gap is much less important and the coupling, as well as the expected LSPR blue shift, much weaker.

For a more quantitative analysis, Figure 4a discloses extinction spectra computed within the discrete dipole approximation (DDA) in the case of perfect cube dimers subjected to a longitudinal excitation and embedded in an effective medium with refractive index $n_{eff} = 1.15$ (see Materials and Methods). The cube side length is 51 nm, and the gap distance d varies from 20 to 0 nm. For an infinite separation, the spectrum is the same as that for an isolated monomer but with a twice larger intensity (Figure 2b). In spite of the fragmentation of the single cube resonance, the LSPR of the pair mainly consists of a broad but single peak that shifts toward the red as the interparticle distance is decreased. The evolution of the LSPR shift is rather slow and does not present any singularity when the contact limit ($d = 0$ nm) is reached, indicating that the far-field optical response of the elongated parallelepiped is not drastically different from the one of two nearly touching perfect cubes. The spectral pattern is less simple for spherical particles of the same volume as illustrated in Figure 4b. Mie calculations have been first carried out since they are straightforward because of the spherical symmetry. When the interparticle distance decreases down to $d = 1$ nm, the spectra show the generic trends highlighted in previous numerical studies.[12,29,43,44] The main resonance of dipolar character (D_S) is shifted to

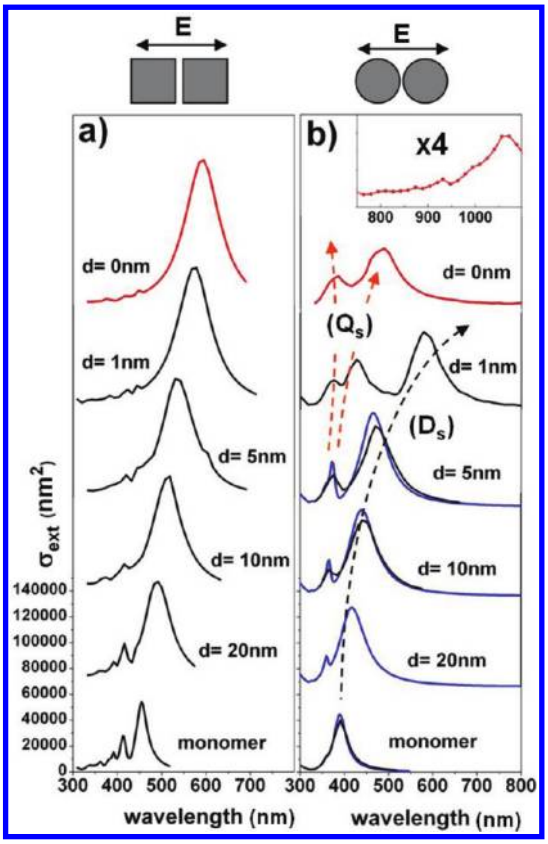

Figure 4. Calculated extinction spectra of perfect silver cube (a) and silver sphere (b) dimers as a function of the interparticle distance *d*. Red curves correspond to the situation of contact ($d = 0$ nm). The particles have the same volume ($L = 51$ nm for cubes and $D = 63$ nm for spheres). DDA and Mie calculations are given by black and blue curves, respectively. The inset in (b) shows the onset of an infrared shifted resonance for two spheres in contact.

the large wavelength side (more rapidly than for cubes) and plasmon contributions of higher order successively grow from the near UV part of the spectrum (quadrupole Q_S) because of their increasing hybridization with the dipolar plasmon mode. In the case of touching spheres ($d = 0$ nm), we have performed DDA calculations since the Mie formalism is not suitable for this highly singular situation. Only high-order multipolar contributions (Q_S) are present in the visible range ($300 \text{ nm} < \lambda < 800$ nm).[45] An additional weak resonance is observed in the infrared range for touching (or overlapping) spheres, but its precise location depends on the extent of the contact area and therefore on the way the cubic dipole array is cut out to reproduce spherical or any curved shape (inset in Figure 4b).

Differences between spectra of touching spheres and spectra of touching cubes are quite illustrative of the influence of capacitive effects on their electrostatic coupling (red curves in Figure 4). When two spherical particles are in contact, the particular geometry of the region delimited by the facing half-spheres favors the development of surface charge distributions with rapid spatial fluctuations and promotes plasmon resonances

of high order in the small wavelength side (top spectrum in Figure 4b). On the other hand, electron cloud oscillation over the whole "dumbbell" dimer is disrupted by charge piling up and by capacitive coupling in the antiwedge region, which induces a strong red shift and a weakening of the dipolar LSPR (inset in the top of Figure 4b). This resonance and the strongly redshifted dipolar LSPR of nontouching spheres (D_S) are not of the same nature, but their vanishing at the singular point-like contact can be explained by a common mechanism.[29] On the other hand, when cubes are brought into contact (d = 0 nm), the volume of the capacitor enclosed by facing squares completely vanishes so as to leave a single and compact parallelepiped. Its optical response is not basically different from the one of a cube, except for a mere change in the aspect ratio. Owing to the large number of dipolar modes for individual cubes and the variety of corresponding surface charge distributions they may sustain[21,36,39,40] (Figure 2e), the local electric field in the gap region between silver cubes has certainly a very complex spatial structure. Surprisingly, the expected singularity of the near-field enhancement during the transition from separated to touching perfect cubes is not reflected in the far-field as shown by the steady evolution of the LSPR with the interparticle distance (Figure 4a).

As it can be seen in Figure 2b and at the cost of an extra broadening of individual resonances, the experimental optical response of a single nanocube is qualitatively well-described by numerical simulations under the hypothesis of a perfectly cubic geometry and without having to introduce edge and corner rounding effects. This also seems to hold for the nanocube dimer D1 in Figure 3a. Figure 5 shows DDA simulations of D1 extinction spectra assuming parallel cube faces and sharp edges (and corners). Other geometrical parameters are obtained from TEM images and are listed in Table 1. The full line spectra are obtained for transverse and longitudinal excitations and an interparticle distance given by TEM (d = d_{app} = 1.75 nm). A good agreement between experiment and theory is obtained by setting the effective refractive index value to n_{eff} = 1.2. It shows here that the optical response of dimer D1 is consistent with the plasmon coupling of cubes that would have perfectly sharp edges. A very similar result is obtained when considering a larger interparticle distance (d = 2.5 nm). This indicates that the LSPR position does not vary rapidly with this parameter, in line with the general trend shown in Figure 4a.

LSPR Splitting in Nonperfect Cube Dimers: Edge Rounding Effects. The observation of two strong resonances for the nanocube dimers D2 and D3 in Figure 3a is quite surprising and, contrary to the above-mentioned case of D1, cannot be explained by the coupling of almost identical perfect cubes even for very small interparticle gaps (Figure 4a). Going beyond the classical electrodynamics by invoking the relevance of the nonlocality of the dielectric function for gap distances shorter than 1 nm would not lead to basically different conclusions since nonlocality is known to rather quench plasmon coupling effects.[46] Moreover, such very small separation distances are certainly unrealistic owing to the size of molecular stabilizers adsorbed on the nanoparticle surface.

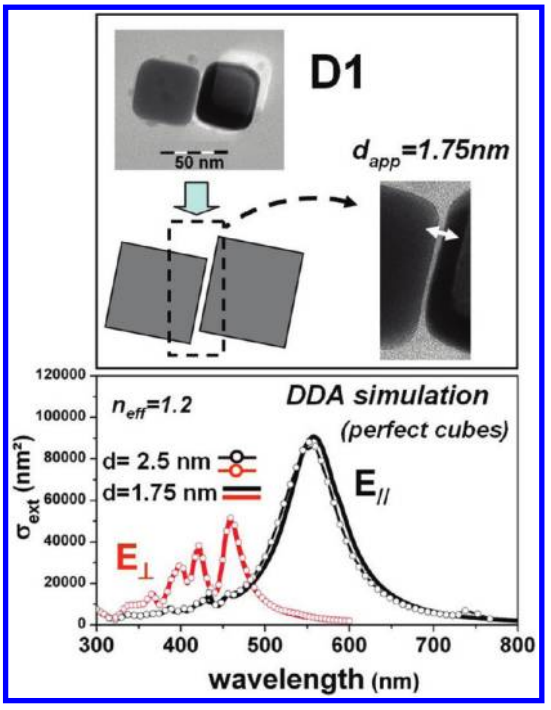

Figure 5. DDA simulations of the extinction spectrum in the case of dimer D1 and under the assumption of perfectly sharp cube edges and corners (see Table 1 for other geometrical parameters). Calculations are made for two different interparticle distances: the value inferred from the TEM image (d = d_{app} = 1.75 nm) and a larger one (d = 2.5 nm).

To account for the LSPR splitting observed in D2 and D3, a very large number of geometrical parameters should be considered in numerical simulations (see Figure 3b). The interparticle distance is crucial, but symmetry breaking could also be invoked to explain new LSPR spectral features and especially the observed splitting. Symmetry breaking may essentially result from changes in the relative orientation of both particles[25−27] or by a size mismatch that appears to be more critical.[20,25] We have then examined their effect in the case of nanocubes and for geometrical distortions consistent with TEM images (selected examples are given in Supporting Information). They are less strong and systematic than those induced by the degree of edge rounding (r_e). We will then focus on the role of this last parameter, restricting ourselves to the case of a longitudinal excitation.

Figure 6a shows the influence of a progressive edge rounding on the extinction spectrum of dimers of

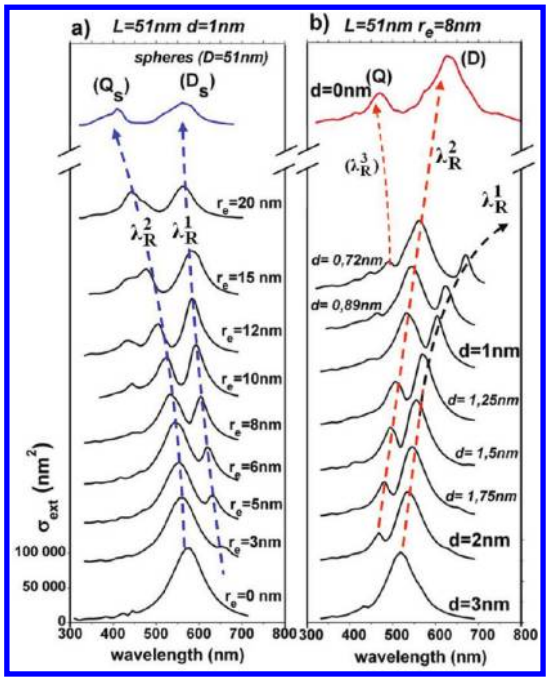

Figure 6. (a) DDA extinction spectra for 51 nm side length cube dimers (interparticle spacing d = 1 nm) as a function of the edge rounding parameter r_e (n_{eff} = 1.15). The top spectrum (blue line) illustrates the case of a dimer of spheres for the same spacing. (b) Calculated extinction spectra for 51 nm side length cube dimers (edge rounding parameter r_e = 8 nm) as a function of the interparticle spacing d. The top spectrum (red line) is obtained for the limit case of touching cubes (d = 0 nm).

identical cubes (L = 51 nm) calculated within the DDA for a fixed separation distance (d = 1 nm). The effective matrix refractive index is arbitrarily set to n_{eff} = 1.15. An additional rounding of the cube corners ($r_c = r_e$ in Figure 1b) would not give significantly different results as well as the choice of an alternative numerical method as FEM (see Figure S4 in Supporting Information). When the rounding is increased, a shoulder (λ_R^1) is growing on the long wavelength side of the initial LSPR. Considering the evolution toward the most smoothed cube geometry (r_e = 20 nm here) and the approximate limit consisting of a pair of perfect spheres, this shoulder clearly develops into what will make up the dipolar resonance for the sphere dimer (D_S). On the other hand, the main resonance of perfect cube dimers (λ_R^2) weakens and further merges with a new resonance on its short wavelength side (r_e > 10 nm) so as to converge toward the group of plasmon resonances of high order for the sphere dimer (Q_S in Figure 4b).

For edge roundings consistent with TEM images (r_e/L = 10−25%), the essential feature is the splitting of the main resonance into two peaks (wavelengths λ_R^1 and λ_R^2). For a qualitative comparison with experiment, we will consider relative shifts $(\lambda_R^1 - \lambda_R^2)/(\lambda_R^1 + \lambda_R^2)$ (or alternatively the ratio λ_R^1/λ_R^2) since these quantities are not too sensitive to the exact values of DDA parameters (n_{eff}, ε_{Ag}, *etc.*) that do not directly characterize the nanocube dimer geometry (see Supporting Information). Although the relative amplitude of both peaks may vary, the ratio λ_R^1/λ_R^2 remains almost constant up to r_e = 12 nm and then increases up to the maximum value given by the ratio of dipolar to quadrupolar-like mode wavelengths ($\lambda_{D_S}/\lambda_{Q_S}$) for the pair of spheres. The key point is that, in the range where both peaks have similar amplitudes, the calculated ratio λ_R^1/λ_R^2 is quite comparable to the one deduced from the experimental spectra of dimers D2 and D3 in Figure 3a. We checked that this observation was quite robust with respect to possible refinements in the nanoparticle dimer description. After having considered the effects of changing the interparticle gap, the particle size, the lateral displacement, the silver dielectric function, the effective matrix refractive index, and even the numerical method (FEM or DDA), one ends up concluding that a splitting into two main resonances is a very general trend, on the necessary conditions that the cube edges are not perfectly sharp but sufficiently rounded and that the distance cube surfaces is small enough (see Supporting Information). For any particular set of parameters (d, r_e) for which both resonances are clearly outlined and of the same order of magnitude, the λ_R^1/λ_R^2 ratio value remains close to 1.15. When the edge rounding is very pronounced and the overall particle shape becomes quasi-spherical, the λ_R^1/λ_R^2 ratio approaches the $\lambda_{D_S}/\lambda_{Q_S}$ limit, which is much more sensitive to the interparticle distance ($\lambda_{D_S}/\lambda_{Q_S}$ = 1.35 for d = 1 and 51 nm diameter spheres).

Another way to investigate the resonance splitting effect is to examine the evolution of optical spectra when cubes with a well-defined edge rounding are now moved close to each other, as illustrated in Figure 6b. For interparticle distances larger than d = 3 nm (not shown here), a single resonance dominates the extinction spectrum and evolves as in the case of perfect cubes (Figure 4a). Down to d = 1 nm, the resonance splits into two peaks labeled λ_R^1 and λ_R^2. In this interparticle distance range, consistent with experimental TEM images, the wavelength ratio λ_R^1/λ_R^2 is still of the order of 1.15. Below d = 1 nm, the spectra evolve more brutally and can be discussed in light of the d = 0 nm case, assuming a continuous evolution of spectra with the interparticle distance. By analogy with what is known for dimers of overlapping spheres,[29] the extinction spectrum at the metallic contact is dominated by two resonances: a large one (D) which is associated to the dipolar electron cloud oscillation over the entire particle pair and a weaker one on its blue side which is related to the appearance of higher order plasmon modes (Q) promoted by the narrowing of the contact region. When the interparticle gap tends to vanish, the resonance (λ_R^2) and a third resonance (λ_R^3) that emerges on its small wavelength side apparently transform into these D and Q resonances, respectively.

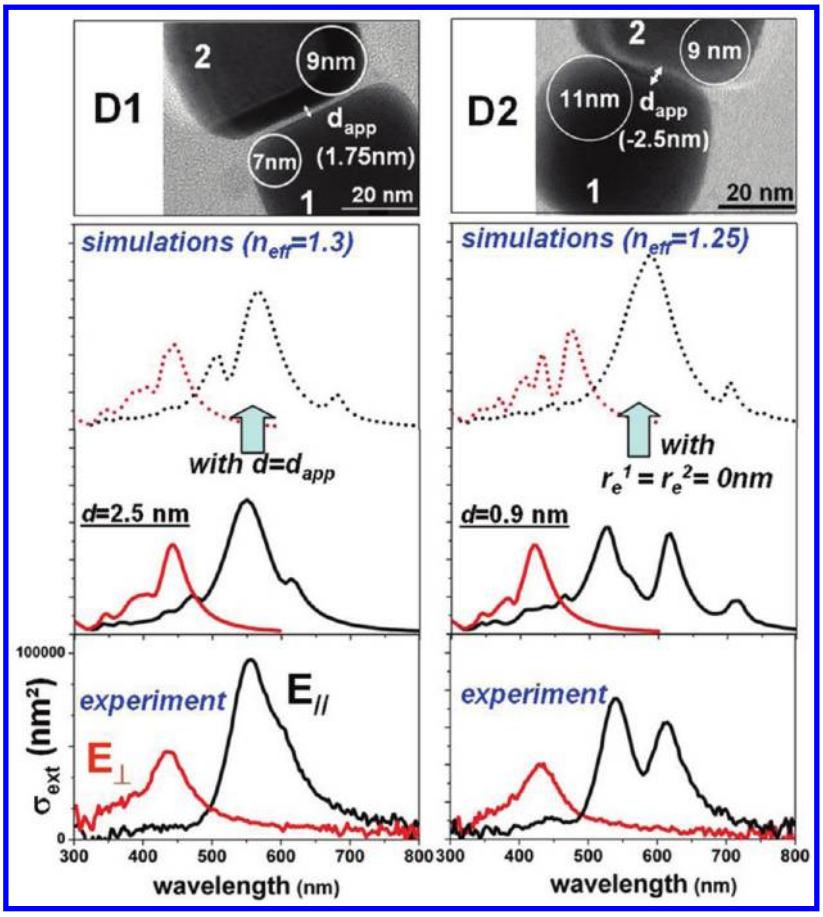

Figure 7. Comparison between experimental and DDA simulated extinction spectra for D1 and D2 nanocube dimers. Individual nanocube geometrical parameters are given in Table 1 and illustrated in the uppermost magnified TEM images. The interparticle distance d and the effective refractive index n_{eff} have been adjusted as free parameters (d = 2.5 nm and n_{eff} = 1.3 for D1, d = 0.9 nm and n_{eff} = 1.25 for D2). The resulting spectra (solid curves) are drawn just above the experimental ones. The dotted line curves show changes in the simulated spectra when some parameters are arbitrarily modified ($d = d_{app}$ for D1 and no edge rounding for D2).

On the other hand, the long wavelength resonance (λ_R^1) is strongly damped and red-shifted, without connection with the spectrum for d = 0 nm, which is flat above λ = 800 nm. It behaves in the same way as the LSPR in dimers of nontouching spheres, which is actually expected to vanish at the point-like conductive contact.[29] From the examination of Figure 6, it may be concluded that the resonance λ_R^1 has a well-defined "dipolar" character as for the main LSPR detected in pairs of spheres. The nature of resonance λ_R^2 (or λ_R^3) is less simply defined, especially for not very smoothed cubes, but clearly turns into higher order plasmon modes of sphere dimers when edge roundings are more pronounced.

On the basis of these calculations, one can infer that, in the case of dimer D1, the relatively large particle separation and the limited edge rounding are not in favor of a splitting of the LSPR. This is why a description in terms of perfect cubes is sufficient in this case. On the contrary, cubes in dimers D2 and D3 are clearly closer and more rounded, which supports the presence of two resonances. Compared to D2, the larger red shift of the longitudinal LSPR for D3 is correlated to a similar shift observed for the perpendicular excitation resonances (Figure 3a). This may be consistent with a larger effective n_{eff} value since the absolute location of LSPR depends not only on the spacing d but also on the exact value of the effective refractive index characterizing the dielectric environment which is known to strongly fluctuate in such systems.[47]

For a more quantitative description, full DDA simulations can be performed by taking advantage of the structural information provided by TEM images. Generally speaking, such simulations are relevant when the number of adjustable parameters required for describing the nanoparticle geometries, properties, and environment is not too large, which is not exactly the case for complex or irregular systems as those shown in Figure 3. Therefore, we have chosen to reproduce D1 and D2 extinction spectra by only adjusting the effective refractive index n_{eff} and the inteparticle distance d. The possibility of a nonperfect parallelism between cube faces has been also considered at the sight of TEM images, and the corresponding Euler angles α (see Figure 3b) are listed in Table 1 together with other

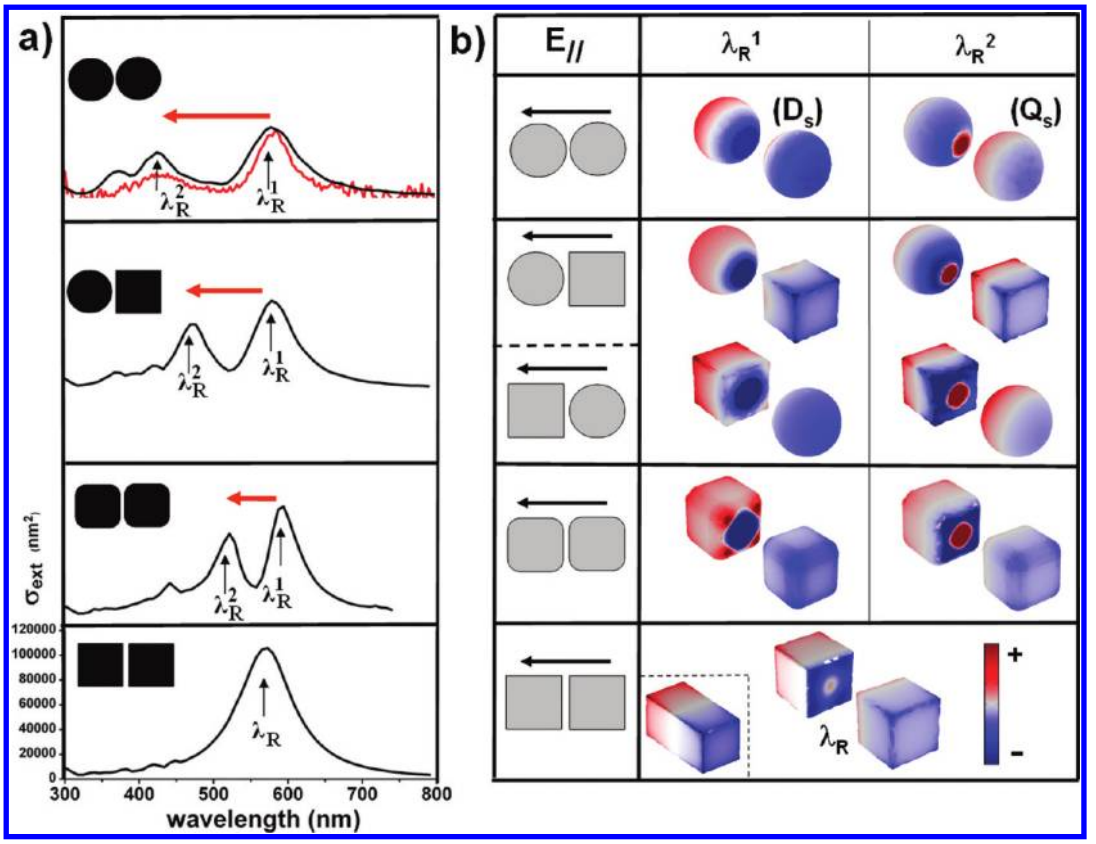

Figure 8. (a) Calculated DDA extinction spectra for a longitudinal excitation in the case of pairs of nanoparticles (d = 1 nm) with different shapes but with the same volume: two spheres, a perfect cube and a sphere, two edge rounded cubes (r_e = 10 nm), and two perfect cubes (51 nm cube side length), from the top to the bottom. The red curve at the top of (a) gives the experimental spectrum measured for a 63 nm diameter sphere dimer (not to scale). (b) Surface charge distributions calculated with FEM at the plasmon resonances λ_R^1, λ_R^2, and λ_R (see Figure 2). For the cube−sphere heterodimer, two perspective views are displayed for inverted nanoparticle positions relative to the exciting electric field $E_{||}$. For quasi-perfect cubes (r_e = 1 nm), the charge distribution of the parallelepiped (top spectrum in Figure 4a) is given in the inset.

geometrical parameters. The results are shown in Figure 7 and compared to the experiment for both polarization directions. Adjusted effective refractive indexes (n_{eff} = 1.25 or 1.3) are larger than the reference value (1.15) previously considered for gold spheres on the same substrate.[48] They are closer to the refractive index of the substrate (n = 1.5), which is not surprising since a larger substrate/nanoparticle contact area is expected in the case of cubes. The interparticle distance is found to be larger for D1 than for D2, which is in line with TEM observations even if the latter may be biased by parallax effects. Beyond the agreement between experiment and simulation, these calculations stress the central role played by cube edge (corner) curvature.

Compared to D2 and D3, cube edge rounding in dimer D1 is slightly less marked but is far from negligible. The satisfying description of D1 extinction spectrum in terms of perfect cube geometries (Figure 5) can thus be simply explained by a relatively large interparticle distance. If this distance is arbitrarily decreased, the residual edge curvature observed in TEM will induce additional structures in the simulated spectrum (dotted lines for $d = d_{app}$ in the left part of Figure 7), which are clearly absent in the experiment. In the same way, neglecting cube edge rounding in dimer D2 leads to a complete vanishing of the LSPR splitting in the simulated spectrum (dotted lines in the right part of Figure 7).

Plasmonic Coupling and Nanoparticle Surface: Curvature Related Effects. Contrary to a sphere, a perfect cube sustains several plasmon modes carrying large electric dipole moments that are efficiently excited by an incident plane wave.[36] Although these modes are no longer degenerated, their coupling in cube pairs surprisingly results in a single red-shifted giant resonance that is very similar to the one induced in dimers of spheres (Figure 4a). Its underlying fine structure cannot be resolved in the case of so large particles. When edges are rounded in the form of quarter cylinders, the volume enclosed by facing surfaces is made of a central square plane capacitor surrounded by four antiwedge regions that can be compared to the curved capacitor interface between perfect spherical particles (radius r_e). The latter will promote surface charge distributions and electrostatic couplings that are not initially allowed in quasi-perfect cube pairs but in dimers of spheres. The role of flat as compared to curved boundaries is illustrated in Figure 8a that shows changes in

extinction spectra for dimers of silver particles having different shapes and face curvatures in the gap region. These particles are perfect cubes, spheres, or edge rounded cubes with a fixed separation (d = 1 nm). The effective matrix refractive index is arbitrarily set to n_{eff} = 1.15 as in Figure 4. The splitting of the LSPR (λ_R^1, λ_R^2) can be observed each time the surface of at least one particle exhibits a curved portion in close proximity of the other particle (see also Supporting Information for heterodimers made of particles with very different sizes).

The ratio λ_R^1/λ_R^2 that measures the magnitude of the LSPR splitting can be considered as the signature of the deviation from a plane interface geometry in the interparticle region. It is all the larger that the antiwedge region is more opened and curved. In the case of the two edge rounded cubes (Figure 8a), λ_R^1/λ_R^2 is of the order of 1.15, which corresponds to the value observed for dimers D2 and D3 in Figure 3a. It is characteristic of antiwedge geometries with a residual central planar region. For a heterodimer made of a cube and a sphere, λ_R^1/λ_R^2 is larger and about 1.25, close to the ratio observed for dimer D4 in Figure 3a. In the case of two spheres, λ_R^1/λ_R^2 is predicted to be more sensitive to the exact value of the interparticle gap as compared to rounded cubes. For the particle size and gap assumed here, it is found close to 1.35. By way of comparison, we also show in the top of Figure 8a the typical experimental extinction spectrum of a dimer of silver spheres with the same volume. Although only low-resolution TEM images can be recorded in that case, the good agreement between both spectra is an indication that the interparticle spacing should be effectively of the order of 1 nm. This seems to be a characteristic distance of near touching nanoparticles chemically synthesized under standard conditions.[12]

Nanoparticle interface effects in the spectral domain can be mirrored by a plasmon mode analysis (FEM). Figure 8b shows the charge distributions that develop on both nanoparticle surfaces at the main resonances. For the dimer of spheres, their expected dipolar (D_S) and quadrupolar (Q_S) symmetries are obvious for λ_R^1 and λ_R^2, respectively (see Figure 4b). For the dimer of perfect cubes, charges with opposite signs are essentially piled up on facing sides, as for a plane capacitor. Contrary to spheres, it is difficult to identify which dipolar modes of the single cube (Figure 2e) may be involved here. The dipolar character of resonance λ_R is supported by the fact that, outside the gap region, the charge distributions on the most distant faces are very similar to what can be calculated for an elongated parallelepiped at its main dipolar resonance (inset in Figure 8b). The case of the heterodimer involving a sphere and a perfect cube is interesting because, for both modes, the surface charge distributions on the sphere are very similar to those of the dimer of spheres. They seem to be simply mirrored by the cubic particle just as if the spherical particle had forced the electrostatic coupling in the gap region. The capacitor made by a half-spherical cap and the cube face has a different geometry compared to the antiwedge previously discussed for the dimer of spheres (Figure 4b), which explains a weaker red shift of the resonance of "quadrupolar" character λ_R^2. In particular, accumulating charges in the vicinity of the interparticle axis is easier on a spherical than a on square face because of a point effect. This point effect can be partly recovered in the case of rounded cubes that have faces made of a central plane square of reduced dimension surrounded by four quarter cylinders. This geometry is less regular than a half-sphere but is all the more similar to it as the edge (corner) rounding is larger. As it can be seen in Figure 8b, the central plane square is able to sustain nodes of the surface charge distributions just like spheres. This explains the evolution of the optical response of cube dimers as a function of edge rounding as evidenced in Figure 6a.

CONCLUSION

In summary, the far-field optical extinction spectroscopy of individual silver nanocube dimers in close coupling configurations has shown evidence for the specific dependence of the LSPR on the nanoparticle shape. As soon as the cube edges (corners) are more or less rounded, the LSPR is split into two distinct resonances. DDA calculations demonstrate that this splitting is mainly due to the degree of cube edge smoothing when the interparticle distance is small enough (1−2 nm). Symmetry breaking effects induced by the deviation of "real" nanocube dimers from the ideal case of pairs of perfectly aligned identical particles may also be responsible of LSPR distortions, but they are neither so pronounced nor systematic. The LSPR splitting is clearly the signature of a change in the geometry of the capacitor delimited by the facing sides of both particles. This local geometry is crucial since it will define the boundary conditions for the development of specific surface charge distributions and the related plasmon oscillation modes. Both new resonances anticipate the "dipolar-like" and "quadrupolar-like" resonances that dominate the spectrum of an ideal dimer of spheres and into which they progressively transform, as the ratio of flat to spherically curved areas at the capacitor boundaries is decreasing. This transition in the frequency domain must find its counterpart in a progressive modification of surface charge and local electromagnetic field distributions at the different resonances, changing from cubic to spherical symmetry. By means of capacitive effects, the antiwedge geometry in the interparticle region will thus control how plasmon resonances of different nature, with regard to the symmetry of induced surface charge distributions, will develop and interact. Small particle

shape distortions are able to modify noticeably the LSPR structure as already discussed in the literature.[49] We show that they are obviously much more critical with regard to the coupling of metallic nanoparticles placed in close proximity. Our experiments demonstrate the possibility of tailoring the optical properties of nanosensors by a precise design of nanoparticle pairs at the near contact limit.

MATERIALS AND METHODS

Synthesis. Silver nanocubes are synthesized by the polyol method using sodium hydrosulfide as described by Siekkinen *et al.*[50] This method is suitable for the study of single isolated nanoparticles because it does not favor their agglomeration in solution. The enhanced formation of dimers can rather be obtained thanks to an alternative technique developed by Li *et al.*[51] with a time reaction of 22 h that favors the assembly of cubic nanoparticles. Colloidal suspensions are further dispersed by spin coating on transparent substrates that are designed for a combined study by optical spectrometry and transmission electron microscopy (TEM). They consist of TEM grids coated with a thin FORMVAR resin film (30 nm thick) which is transparent in the visible range (refractive index about 1.5) and resistant to electron irradiation in TEM. In contrast with nanoparticle pairs designed from nanolithography techniques, very small interspacing distances can be explored here by taking advantage of steric effects due to the residual layer of surfactant molecules at the metal surface.[12]

Optical and Electron Microscopies. The absolute extinction cross section of single nanoparticles or nanoparticle pairs is measured in the 300−800 nm range by the spatial modulation spectroscopy (SMS) technique described in previous papers.[48,52] It consists of irradiating a supported particle by the light beam provided by a quartz tungsten halogen lamp and focused at the diffraction limit by a high aperture reflecting objective. The transmitted light is dispersed by a monochromator and measured by a photomultiplier device. A sine displacement (frequency f) is applied to one axis of a high-resolution XY piezoelectric stage so as a given particle periodically enters in and out the light beam. The subsequent modulation of the transmitted light is detected by a lock-in amplifier at frequency f (or $2f$) which greatly improves the signal-to-noise ratio. The ratio of the lock-in signal to the DC transmitted light signal is converted into an absolute extinction cross section thanks to a previous characterization of the beam spot profile in the focal plane. The average particle density on the substrate is less than 1 μm^{-2} in such a way that only one object is irradiated by the focused light beam at any time. Transmission electron microscopy (TEM) images are recorded after the complete optical study since the supporting film can be strongly heated by the electron beam and altered in the close vicinity of the nanoparticle, possibly modifying its intrinsic optical response. TEM analysis gives access not only to the shape of the particles, projected in the substrate plane, but also to their orientation relative to the direction of light polarization in SMS measurements (dimer axis for instance). Optical measurements are performed with linearly polarized light thanks to a broad band polarizing cube placed on a rotating mount at the entrance of the spectrometer. In the case of anisotropic objects (nanoparticle pairs for instance), the spectra are recorded for two orthogonal directions of light polarization, adjusted so as to obtain a maximum difference in the spectral location of the LSPR. In view of the orientation of the projected TEM images relative to the frame of the optical setup, both directions are proven to correspond to the long and short symmetry axes of each pair, with an accuracy of $\pm 3°$. TEM observations confirm that particles have grown as cubes with not perfectly sharp but more or less rounded edges. The geometrical structure of three-dimensional nanoparticles cannot be fully deduced from conventional TEM images. Some dimensions have to be assumed on reasonable grounds (particle height, curvatures of edges parallel to the substrate, *etc.*).

Calculations. Extinction cross sections are essentially calculated within the discrete dipole approximation, by using the code (version DDSCAT 7.0) developed by Draine and Flatau.[53,54] Considering the size of nanocubes synthesized here (L = 40−50 nm) and an upper limit for the computing time, the mesh size of the square dipole array has been set to 1 nm (10^5 to 1.5×10^5 dipoles per nanoparticle). For parallel cubes, the distance d_i between flat faces is given by the number of unoccupied dipole cells and will correspond to an integer number of elementary spacings ($d_i = i$ nm). Noninteger mesh sizes and d_{ni} values ($d_{i-1} < d_{ni} < d_i$) can nevertheless be considered just by representing a cubic particle with volume L^3 (nm^3) by a cubic array of $L' \times L' \times L'$ dipoles, with the condition $L' = Ld_i/d_{ni}$. For ensuring a more convenient handling of the dipole arrays generated by a home-built code, according to the mesh size prescription described above, the nanocube dimensions measured by TEM are conveniently rounded off. Generally speaking, it should be underlined that DDA calculations have to be considered cautiously, at least on quantitative grounds, for situations where the minimum distance between dipoles belonging to different particles becomes of the same order as the mesh size. The dielectric function of silver nanoparticles ε_{Ag} is taken as that of bulk silver from the Johnson and Christy table[55] without phenomenological correction for size reduction effects. Symmetry breaking introduced by the air−dielectric substrate interface is not taken into account explicitly in this paper. The particles are assumed to be embedded in a homogeneous dielectric background which is described by an effective refractive index labeled n_{eff}, intermediate between the air and the thin supporting film indices (n = 1 and $n \cong 1.5$, respectively).[4] In most of the calculations and as inferred from previous studies on spherical gold particles supported on the same substrate,[48] we will choose the value n_{eff} = 1.15 as a reference. In the case where precise adjustments between experiment and theory are needed, n_{eff} will be treated as a fitting parameter around this reference value.

We also performed finite element method (FEM) simulations using the RF module of the COMSOL 4.1 commercial software. DDA and FEM are complementary numerical techniques. DDA is less sensitive than FEM to spatial singularities when defining the geometry of nanoparticles. It is more suitable to treat sharp edges, corners, and wedges for instance. On the other hand, spurious effects related to the finite size of the dipole arrays in DDA and the induced surface roughness are minimized in FEM. Additional Mie calculations are made using a home-built code based on a conventional multiple scattering approach (generalized Mie theory).[56,57]

Acknowledgment. The authors acknowledge the technical assistance from the staff of the NanOptec Center facility in the University of Lyon 1. One of us (M.B.) thanks the "Institut Universitaire de France (IUF)" for financial support.

Supporting Information Available: DDA calculations of asymmetric silver nanocube dimers: (i) aligned cubes of different sizes and edge roundings (Figure S1), (ii) misaligned cubes of the same size but different edge roundings (Figure S2). Effects of corner rounding and comparison between DDA and FEM calculations, for single nanocubes (Figure S3) and for nanocube dimers (Figure S4). Effect of the external medium refractive index on the LSPR splitting of edge rounded nanocube dimers (Figure S5). FEM calculations and simulations of experimental extinction spectra for selected nanocube dimers (Figure S6). This material is available free of charge *via* the Internet at http://pubs.acs.org.

REFERENCES AND NOTES

1. Bohren, C. F.; Huffman, D. P. *Absorption and Scattering of Light by Small Particles*; Wiley: New York, 1983.
2. Hao, E.; Schatz, G. C. Electromagnetic Fields around Silver Nanoparticles and Dimers. *J. Chem. Phys.* **2004**, *120*, 357–366.
3. Encina, E. R.; Perassi, E. A.; Coronado, E. A. Near-Field Enhancement of Multipole Plasmon Resonances in Ag and Au Nanowires. *J. Phys. Chem. A* **2009**, *113*, 4489–4497.
4. Kreibig, U.; Vollmer, M. *Optical Properties of Metal Clusters*; Springer: Berlin, 1995.
5. McFarland, A. D.; Duyne, R. P. V. Single Silver Nanoparticles as Real-Time Optical Sensors with Zeptomole Sensitivity. *Nano Lett.* **2003**, *3*, 1057–1062.
6. Vo-Dinh, T.; Dhawan, A.; Norton, S. J.; Khoury, C. G.; Wang, H. N.; Misra, V.; Gerhold, M. D. Plasmonic Nanoparticles and Nanowires: Design, Fabrication and Application in Sensing. *J. Phys. Chem. C* **2010**, *114*, 7480–7488.
7. Zhao, J.; Das, A.; Schatz, G. C.; Sligar, S. G.; Van Duyne, R. P. Resonance Localized Surface Plasmon Spectroscopy: Sensing Substrate and Inhibitor Binding to Cytochrome P450. *J. Phys. Chem. C* **2008**, *112*, 13084–13088.
8. Atay, T.; Song, J.-H.; Nurmikko, A. V. Strongly Interacting Plasmon Nanoparticles Pairs: From Dipole−Dipole Interaction to Conductively Coupled Regime. *Nano Lett.* **2004**, *4*, 1627–1631.
9. Gunnarsson, L.; Rindzevivius, T.; Prikulis, J.; Kasemo, B.; Käll, M.; Zou, S.; Schatz, G. C. Confined Plasmons in Nanofabricated Single Silver Particle Pairs: Experimental Observations of Strong Interparticle Interactions. *J. Phys. Chem. B* **2005**, *109*, 1079–1087.
10. Muskens, O. L.; Giannini, V.; Sanchez-Gil, J. A.; Rivas, J. G. Optical Scattering Resonances of Single and Coupled Dimer Plasmonic Nanoantennas. *Opt. Express* **2007**, *15*, 17736–17746.
11. Su, K. H.; Wei, G. H.; Zhang, X.; Mock, J. J.; Smith, D. R.; Schultz, S. Interparticle Coupling Effects on Plasmon Resonances of Nanogold Particles. *Nano Lett.* **2003**, *3*, 1087–1090.
12. Marhaba, S.; Bachelier, G.; Bonnet, C.; Broyer, M.; Cottancin, E.; Grillet, N.; Lermé, J.; Vialle, J.-L.; Pellarin, M. Surface Plasmon Resonance of Single Gold Nanodimers near the Conductive Contact Limit. *J. Phys. Chem. C* **2009**, *113*, 4349–4356.
13. Tabor, C.; Murali, R.; Mahmoud, M.; El-Sayed, M. A. On the Use of Plasmonic Nanoparticle Pairs as a Plasmon Ruler: The Dependence of the Near-Field Dipole Plasmon Coupling on Nanoparticle Size and Shape. *J. Phys. Chem. A* **2009**, *113*, 1946–1953.
14. Sönnichsen, C.; Reinhard, B. M.; Liphardt, J.; Alivisatos, A. P. A Molecular Ruler Based on Plasmon Coupling of Single Gold and Silver Nanoparticles. *Nat. Biotechnol.* **2005**, *23*, 741–745.
15. Nordlander, P.; Halas, N. J.; Lal, S.; Chang, W. S.; Link, S. Plasmons in Strongly Coupled Metallic Nanostructures. *Chem. Rev.* **2011**, *111*, 3913–3961.
16. Ringler, M.; Schwemer, A.; Wunderlich, M.; Nichtl, A.; Kürzinger, K.; Klar, T. A.; Feldmann, J. Shaping Emission Spectra of Fluorescent Molecules with Single Plasmonic Nanoresonators. *Phys. Rev. Lett.* **2008**, *100*, 203002.
17. Dadosh, T.; Sperling, J.; Bryant, G. W.; Breslow, R.; Shegai, T.; Dyshel, M.; Haran, G.; Bar-Joseph, I. Plasmonic Control of the Shape of the Raman Spectrum of a Single Molecule in a Silver Nanoparticle Dimer. *ACS Nano* **2009**, *3*, 1988–1994.
18. Hatab, N. A.; Hsueh, C. H.; Gaddis, A. L.; Retterer, S. T.; Li, J. H.; Eres, G.; Zhang, Z. Y.; Gu, B. H. Free-Standing Optical Gold Bowtie Nanoantenna with Variable Gap Size for Enhanced Raman Spectroscopy. *Nano Lett.* **2010**, *10*, 4952–4955.
19. Acimovic, S.; Kreuzer, M. P.; Gonzalez, M. U.; Quidant, R. Plasmon Near-Field Coupling in Metal Dimers as a Step toward Single-Molecule Sensing. *ACS Nano* **2009**, *5*, 1231–1237.
20. Brown, L. V.; Sobhani, H.; Lassiter, J. B.; Nordlander, P.; Halas, N. J. Heterodimers: Plasmonic Properties of Mismatched Nanoparticle Pairs. *ACS Nano* **2010**, *4*, 819–832.
21. Mahmoud, M. A.; Snyder, B.; El-Sayed, M. A. Surface Plasmon Fields and Coupling in the Hollow Gold Nanoparticles and Surface-Enhanced Raman Spectroscopy. Theory and Experiment. *J. Phys. Chem. C* **2010**, *114*, 7436–7443.
22. Hentschel, M.; Saliba, M.; Vogelgesang, R.; Giessen, H.; Alivisatos, A. P.; Liu, N. Transition from Isolated to Collective Modes in Plasmonic Oligomers. *Nano Lett.* **2010**, *10*, 2721–2726.
23. Habteyes, T. G.; Dhuey, S.; Cabrini, S.; Schuck, P. J.; Leone, S. R. Theta-Shaped Plasmonic Nanostructures: Bringing "Dark" Multipole Plasmon Resonances into Action *via* Conductive Coupling. *Nano Lett.* **2011**, *11*, 1819–1825.
24. Xia, Y. N.; Rycenga, M.; Cobley, C. M.; Zeng, J.; Li, W. Y.; Moran, C. H.; Zhang, Q.; Qin, D. Controlling the Synthesis and Assembly of Silver Nanostructures for Plasmonic Applications. *Chem. Rev.* **2011**, *111*, 3669–3712.
25. Slaughter, L. S.; Wu, Y. P.; Willingham, B. A.; Nordlander, P.; Link, S. Effects of Symmetry Breaking and Conductive Contact on the Plasmon Coupling in Gold Nanorod Dimers. *ACS Nano* **2010**, *4*, 4657–4666.
26. Tabor, C.; Van Haute, D.; El-Sayed, M. A. Effect of Orientation on Plasmonic Coupling between Gold Nanorods. *ACS Nano* **2009**, *3*, 3670–3678.
27. Funston, A. M.; Novo, C.; Davis, T. J.; Mulvaney, P. Plasmon Coupling of Gold Nanorods at Short Distances and in Different Geometries. *Nano Lett.* **2009**, *9*, 1651–1658.
28. Perez-Gonzalez, O.; Zabala, N.; Borisov, A. G.; Halas, N. J.; Nordlander, P.; Aizpurua, J. Optical Spectroscopy of Conductive Junctions in Plasmonic Cavities. *Nano Lett.* **2010**, *10*, 3090–3095.
29. Romero, I.; Aizpurua, J.; Bryant, G. W.; Garcia de Abajo, F. J. Plasmons in Nearly Touching Metallic Nanoparticles: Singular Response in the Limit of Touching Dimers. *Opt. Express* **2006**, *14*, 9988–9999.
30. Mahmoud, M. A.; Tabor, C. E.; El-Sayed, M. A. Surface-Enhanced Raman Scattering Enhancement by Aggregated Silver Nanocube Monolayers Assembled by the Langmuir−Blodgett Technique at Different Surface Pressures. *J. Phys. Chem. C* **2009**, *113*, 5493–5501.
31. Sosa, I. O.; Noguez, C.; Barrera, R. G. Optical Properties of Metal Nanoparticles with Arbitrary Shapes. *J. Phys. Chem. B* **2003**, *107*, 6269–6275.
32. Zhou, F.; Li, Z. Y.; Liu, Y.; Xia, Y. N. Quantitative Analysis of Dipole and Quadrupole Excitation in the Surface Plasmon Resonance of Metal Nanoparticles. *J. Phys. Chem. C* **2008**, *112*, 20233–20240.
33. Cobley, C. M.; Skrabalak, S. E.; Campbell, D. J.; Xia, Y. A. Shape-Controlled Synthesis of Silver Nanoparticles for Plasmonic and Sensing Applications. *Plasmonics* **2009**, *4*, 171–179.
34. Fuchs, R. Theory of the Optical Properties of Ionic Crystal Cubes. *Phys. Rev. B* **1975**, *11*, 1732–1739.
35. Langbein, D. Normal Modes at Small Cubes and Rectangular Particles. *J. Phys. A: Math. Theor.* **1976**, *9*, 627–644.
36. Zhang, S. P.; Bao, K.; Halas, N. J.; Xu, H. X.; Nordlander, P. Substrate-Induced Fano Resonances of a Plasmonic: Nanocube: A Route to Increased-Sensitivity Localized Surface Plasmon Resonance Sensors Revealed. *Nano Lett.* **2011**, *11*, 1657–1663.
37. Sherry, L. J.; Chang, S.-H.; Schatz, G. C.; Van Duyne, R. P.; Wiley, B. J.; Xia, Y. Localized Surface Plasmon Resonance Spectroscopy of Single Silver Nanocubes. *Nano Lett.* **2005**, *5*, 2034–2038.
38. McMahon, J. M.; Wang, Y.; Sherry, L. J.; Van Duyne, R. P.; Marks, L. D.; Gray, S. K.; Schatz, G. C. Correlating the Structure, Optical Spectra, and Electrodynamics of Single Silver Nanocubes. *J. Phys. Chem. C* **2009**, *113*, 2731–2735.
39. Lee, S. Y.; Hung, L.; Lang, G. S.; Cornett, J. E.; Mayergoyz, I. D.; Rabin, O. Dispersion in the SERS Enhancement with Silver Nanocube Dimers. *ACS Nano* **2010**, *4*, 5763–5772.
40. Kim, D. S.; Heo, J.; Ahn, S. H.; Han, S. W.; Yun, W. S.; Kim, Z. H. Real-Space Mapping of the Strongly Coupled Plasmons of Nanoparticle Dimers. *Nano Lett.* **2009**, *9*, 3619–3625.

41. Huanjun, C.; Zhenhua, S.; Weihai, N.; Choi, W. K.; Hai-Qing, L.; Lingdong, S.; Chunhua, Y.; Jianfang, W. Plasmon Coupling in Clusters Composed of Two-Dimensionally Ordered Gold Nanocubes. *Small* **2009**, *5*, 2111–2119.
42. Prodan, E; Nordlander, P. Plasmon Hybridization in Spherical Particles. *J. Chem. Phys.* **2004**, *120*, 5444–5454.
43. Encina, E. R.; Coronado, E. A. Plasmon Coupling in Silver Nanosphere Pairs. *J. Phys. Chem. C* **2010**, *114*, 3918–3923.
44. Nordlander, P.; Oubre, C.; Prodan, E.; Li, K.; Stockman, M. I. Plasmon Hybridization in Nanoparticle Dimers. *Nano Lett.* **2004**, *4*, 899–903.
45. The generation of a cubic array of individual dipoles inside a spherical envelope systematically leads to truncation effects and to a spurious surface granularity which explains the deviations of DDA as compared to Mie calculations when the particle separation is approaching the surface roughness scale.
46. Garcia de Abajo, F. J. Nonlocal Effects in the Plasmons of Strongly Interacting Nanoparticles, Dimers, and Waveguides. *J. Phys. Chem. C* **2008**, *112*, 17983–17987.
47. Muskens, O. L.; Billaud, P.; Broyer, M.; Del Fatti, N.; Vallée, F. Optical Extinction Spectrum of a Single Metal Nanoparticle: Quantitative Characterization of a Particle and of Its Local Environment. *Phys. Rev. B* **2008**, *78*, 205410.
48. Billaud, P.; Marhaba, S.; Cottancin, E.; Arnaud, L.; Bachelier, G.; Bonnet, C.; Del Fatti, N.; Lermé, J.; Vallée, F.; Vialle, J.-L.; Broyer, M.; Pellarin, M. Correlation between the Extinction Spectrum of a Single Metal Nanoparticle ant Its Electron Microscopy Image. *J. Phys. Chem. C* **2008**, *112*, 978–982.
49. Goldys, A. M.; Calander, N.; Drozodowicz-Tomsia, K. Extreme Sensitivity of the Optical Properties of Metal Nanostructures to Minor Variations in Geometry Is Due to Highly Localized Electromagnetic Field Forces. *J. Phys. Chem. C* **2010**, *115*, 676–682.
50. Siekkinen, A. R.; McLellan, J. M.; Chen, J. Y.; Xia, Y. N. Rapid Synthesis of Small Silver Nanocubes by Mediating Polyol Reduction with a Trace Amount of Sodium Sulfide or Sodium Hydrosulfide. *Chem. Phys. Lett.* **2006**, *432*, 491–496.
51. Li, W.; Camargo, P. H. C.; Lu, X.; Xia, Y. Dimers of Silver Nanospheres: Facile Synthesis and Their Use as Hot Spots for Surface-Enhanced Raman Scattering. *Nano Lett.* **2009**, *9*, 485–490.
52. Billaud, P.; Marhaba, S.; Grillet, N.; Cottancin, E.; Bonnet, C.; Lermé, J.; Vialle, J.-L.; Broyer, M.; Pellarin, M. Absolute Optical Extinction Measurements of Single Nano-Objects by Spatial Modulation Spectroscopy Using a White Lamp. *Rev. Sci. Instrum.* **2010**, *81*, 043101.
53. Draine, B. T.; Flatau, P. J. Discrete-Dipole Approximation for Scattering Calculations. *J. Opt. Soc. Am. A* **1994**, *11*, 1491–1499.
54. Draine, B. T.; Flatau, P. J. User Guide for the Discrete Dipole Approximation Code DDSCAT 7.0; http://arxiv.org/abs/0809.0338, 2008.
55. Johnson, P. B.; Christy, R. W. Optical Constants of the Noble Metals. *Phys. Rev. B* **1972**, *6*, 4370–4379.
56. Mishchenko, M. I.; Travis, L. D.; Lacis, A. A. *Scattering, Absorption, and Emission of Light by Small Particles*; Cambridge University Press: Cambridge, 2002.
57. Gerardy, J. M.; Ausloos, M. Absortpion Spectrum of Clusters of Spheres from the General Solution of Maxwell's Equation. II. Optical Properties of Aggregated Metal Spheres. *Phys. Rev. B* **1981**, *25*, 4204–4229.